Characterization and stabilization of the unstable fixed points of a frequency doubled Nd:YAG laser

A. Schenck zu Schweinsberg and U. Dressler
DaimlerChrysler AG, Research and Technology, Goldsteinstraße 235, D-60528 Frankfurt, Germany
(Received 20 November 2000; published 19 April 2001)

We demonstrate the successful stabilization of type II chaos of a multimode, intracavity frequency doubled, diode-pumped Nd:YAG (neodymium-doped yttrium aluminum garnet) laser in experiment using an adaptive proportional feedback control. The two orthogonal polarized infrared intensities are fed back to the injection current of the pump diode. The stability properties of the stabilized unstable fixed points are investigated and exploited to explain the performance of our control scheme and to determine suitable measurement signals for the feedback control.

DOI: 10.1103/PhysRevE.63.056210 PACS number(s): 05.45.−a

I. INTRODUCTION

Intracavity frequency doubling of continuous wave (CW) solid-state lasers is demonstrated to be an efficient method to transform the fundamental infrared laser radiation into visible radiation by the processes of second harmonic and sum frequency generation. Pumping these lasers with CW laser diodes allows a further improvement of second harmonic output power and efficiency. However, the multimode operation of such lasers develops emission instabilities known as the *green problem* [1]. These instabilities are due to the global coupling of the fundamental modes through the sum frequency generation in the nonlinear crystal. Therefore the occurrence of deterministic chaos is possible and is observed at high pump levels.

The chaotic laser intensities were analyzed in [2] with respect to their nonlinear dynamics. Abarbanel *et al.* observed two general classes of chaotic behavior. They labeled the laser dynamics *type I chaos* when all infrared laser modes are polarized parallel to each other. In this state the production of green light is small. For the second class of chaotic behavior which they called *type II chaos* fundamental modes in both orthogonal eigenpolarization directions x and y of the laser are present. In this latter case the production of green light is much stronger. Therefore type II chaos is more relevant for technical applications than type I chaos.

There exist different *optical* solutions for the green problem, such as single frequency operation or external frequency doubling (for an overview see [3]). However, these solutions increase the complexity of the optical setup. A different approach to suppress the undesired fluctuations was proposed by Roy *et al.* [4] applying an electronic feedback control to the injection current of the pump diode. They implement the occasional proportional feedback (OPF) method [5] that is related [6] to the well-known Ott-Grebogi-Yorke approach [7] for controlling chaos. Both methods consist of applying *time-discrete* feedback control to stabilize unstable periodic orbits lying in a chaotic attractor. Feeding the total infrared intensity S_{tot} back to the injection current of the pump diode, Roy *et al.* succeeded in stabilizing periodic orbits starting from chaotic fluctuations belonging to class I. In [8,9] the same method was applied to stabilize steady-state solutions, too. Moreover, numerical simulations of the OPF method [10] and an extension [11] of the method was performed on rate equations for the intracavity frequency doubled laser.

So far, the experimental stabilization of steady states in [8,9] was only possible for type I chaos. The technically more important case of type II chaos could not be stabilized. In this paper we apply a *time-continuous* feedback control to stabilize steady states also for type II chaos. We take the infrared intensity S_{tot} and split it up in the two infrared intensities S_x and S_y each polarized in one of the orthogonal eigenpolarization directions of the laser. The controller consists of two proportional elements applied to these intensities. The sum of the proportional elements is then fed back to the injection current of the laser diode. This feedback strategy has been studied analytically and numerically in [12] on the rate equations of the laser.

Now, the main focus of our paper is not the feedback control itself but the analysis that follows the stabilization of the fixed points. We investigate the stability properties of the fixed points we were able to stabilize. It turns out that the stable and unstable subspace of these fixed points obey general properties that become evident when the two intensities S_x and S_y are taken as measurement signals. The determination of the unstable direction in the S_x-S_y plane reveals that the total infrared intensity $S_{\mathrm{tot}}=S_x+S_y$ is not well suited to be used in a feedback control that again explains the failure in [8,9] to stabilize type II chaos. In addition, the determination of the influence of the injection current on the location of the fixed points shows that the injection current is very problematic to be used as control parameter. Furthermore, the result of our analysis of the stability properties can be exploited to choose the proportionality factors of the feedback loop.

Our paper is organized as follows. In the next section the experimental setup is described. In Sec. III the feedback control is presented. In the main Sec. IV we characterize in detail the stability properties of the steady-state solutions and give the resulting consequences for suitable measurement quantities for a feedback control approach. In Sec. V the choice of the proportionality factors of the feedback loop is described. Two methods are presented. One is based on the results of Sec. IV, the second one uses the simulated annealing optimization. Finally in Sec. VI we summarize and highlight some conclusions.

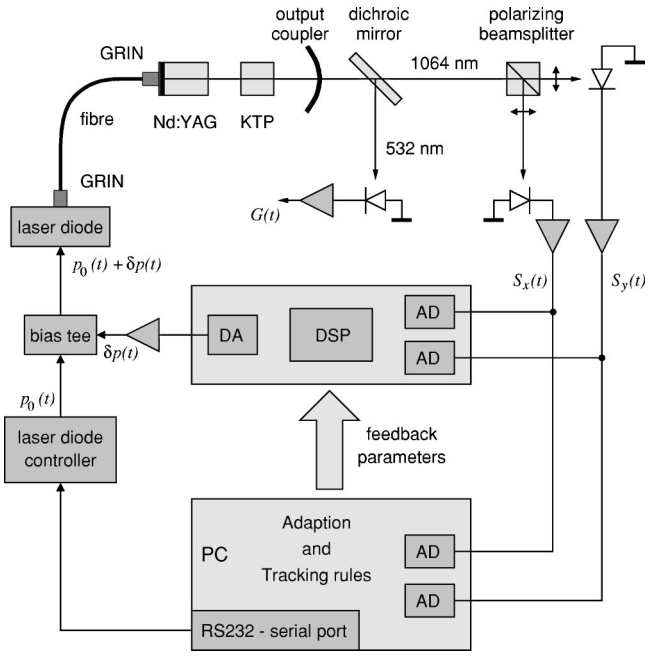

FIG. 1. Experimental setup. The Nd:YAG crystal is end-pumped by a laser diode. The spherical output coupler is highly reflecting at the fundamental wavelength and transmitting at the frequency doubled wavelength. The dichroic mirror reflects the frequency doubled and transmits the fundamental beam. Using a polarizing beamsplitter the latter one is divided into two orthogonal polarized waves that are separately detected and sampled by two AD converters of a digital signal processor (DSP) board. The DSP calculates an appropriate control signal that is transmitted via a DA converter to a bias tee. Via this bias tee, the amplified control signal modulates the current of the pump diode supplied by the laser diode controller. In order to adapt the parameter of the DSP controller, a personal computer observes the intensities using a data aquisition board with two AD converters.

II. EXPERIMENTAL SETUP

Our studies have been performed with the intracavity doubled Nd:YAG (neodymium-doped yttrium aluminum garnet) laser shown in Fig. 1. The Nd:YAG crystal is pumped by a laser diode emitting at $\sim$808 nm. The divergent pump beam is focused into a fiber by a GRIN (gradient index) lens, a second GRIN lens on the opposite of the fiber focuses the pump beam into the cylindrical YAG rod. The flat front face of the Nd:YAG crystal is highly reflecting at the fundamental (1064 nm) and frequency-doubled (532 nm) wavelength and highly transmitting at the pump wavelength. The output coupler has a 500 mm radius of curvature and is transmitting at the doubled frequency and reflecting ($R>99.8\%$) at the fundamental. The laser cavity of length 100 mm contains a nonlinear KTP (potassium titanyl phosphate) crystal that serves as frequency doubling element. It is anti-reflection coated at 1064 nm and 532 nm. Due to the birefringence of the type II phase matched KTP crystal each cavity mode exists in one of two orthogonal eigenpolarization directions that we label x and y direction.

A dichroic mirror is placed behind the output coupler to separate the radiation at 532 nm and 1064 nm. The frequency doubled (green) beam is reflected and is detected by a photodiode with amplifier. The correspondig intensity is called $G(t)$. Using a polarizing beamsplitter the transmitted infrared beam at 1064 nm is subsequently divided into two orthogonal polarized waves corresponding to the two eigenpolarization directions x and y. Both infrared intensities $S_x(t)$ and $S_y(t)$ are detected by photodiodes and amplified.

The lasing threshold of the Nd:YAG laser was obtained at 40 mW pump power P_{thr} of the laser diode corresponding to an injection current of about 700 mA. From the physical point of view it is more interesting to look at the pump rate $r=P/P_{\mathrm{thr}}$. For our system we have found, that the relation

$$r \approx \frac{0.015}{\mathrm{mA}} p - 9.5 \tag{1}$$

between the pump rate r and the injection current p is a good approximation.

In order to stabilize the laser the output voltages of the amplifiers that correspond to the intensities $S_x(t)$ and $S_y(t)$ are sampled using two analog digital (AD) converters with a resolution of 12 bit. The 40-MHz digital signal processor (DSP) calculates the control signal $\delta p(t)$ as a function of the sampled intensities $S_x(t)$ and $S_y(t)$. The 12-bit digital analog (DA) converter has as output a voltage proportional to the control signal δp that modulates the injection current p_0 of the pump diode via a bias tee with a low-pass frequency of 500 Hz.

The realization of the feedback using a DSP and AD/DA converters has the advantage that different control methods can be tested with only little effort. But the drawback of this approach is a time lag of the output of the control signal resulting from conversion and calculation time. In our setup the time lag is around 3 μs and therefore small in comparison with the typical frequencies of the output intensities that are on the order of 30 kHz.

To observe the evolution of the intensities during control, two additional AD converters triggered by a personal computer are used. They are necessary to adapt the parameters of the feedback control to drifting system parameters as discribed in Sec. V.

III. THE ADAPTIVE CONTROL METHOD

We have tested different control strategies like the OPF control [5], (extended) time delayed autosynchronization [13,14], or simple proportional feedback control. The latter one which we present in Eq. (2) has shown the best results in stabilizing and adapting the control to drifting system parameters. So, we restrict ourself in this paper to the following control method.

To stabilize an unstable fixed point we use proportional feedback of the two orthogonal polarized intensities S_x and S_y that we feed back to the injection current p of the pump diode, i.e.,

$$\delta p(t) = k_x[S_x(t) - S_x^0] + k_y[S_y(t) - S_y^0], \tag{2}$$

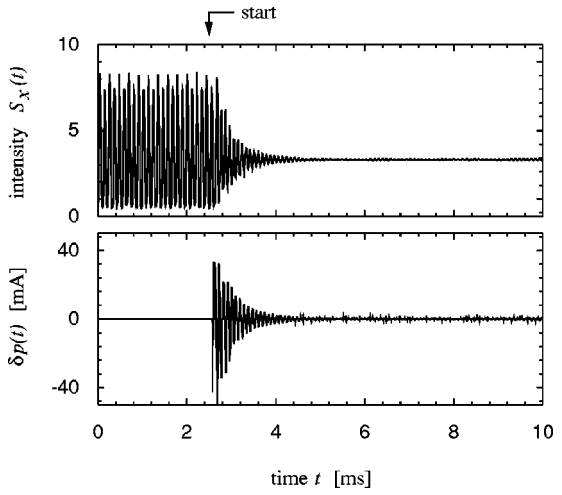

FIG. 2. Stabilization of the laser in a chaotic state. The measurement signal S_x and the control signal δp shows the start of the control and the stabilization of a fixed point.

with S_x^0 and S_y^0 being the intensities corresponding to the unstable steady state to be stabilized.

As the position of the unstable fixed point is usually not known, we have four unknown parameters in the control formula, namely, S_x^0, S_y^0 and k_x, k_y. Our ansatz for estimating the position $\mathbf{S}^0=(S_x^0,S_y^0)$ of the fixed point is

$$S_{x/y}^0 \approx \langle S_{x/y}(t)\rangle = \frac{1}{T}\int_{t-T}^{t} S_{x/y}(s)ds, \tag{3}$$

i.e., we do a moving average of the intensities that is roughly the same as a low-pass filter. This approach can be viewed as an automatic search of the steady-state values S_x^0 and S_y^0. In Fig. 2 the stabilization of an unstable fixed point using the control formula (2) is shown.

In our experiment, it turns out that Eq. (3) is indeed a very good approximation of the location of the unstable fixed points. To quantify the difference between the averages (3) of the uncontrolled system and the steady-state values S_x^0,S_y^0 obtained after stabilization we use the relative error

$$E=\frac{\sqrt{[\langle S_x(t)\rangle - S_x^0]^2+[\langle S_y(t)\rangle - S_y^0]^2}}{S_{\mathrm{tot}}^0}. \tag{4}$$

In Fig. 3 a histogram of E calculated from 58 stabilized unstable fixed points is shown. We observe that in most cases the averages (3) of the uncontrolled system estimate amazingly well the intensities of the steady-state solution after stabilization. This fact was already described in [8] for the total infrared intensity. In [9] the average of the total infrared intensity was applied as reference level in the OPF method to stabilize the steady-state solution of a frequency doubled Nd:YAG laser.

We note that we also have tried to estimate the position of the unstable fixed point by analyzing chaotic time series of the laser intensities. The well-known method of recurrence points [15,16] was applied in a reconstructed state space, but without satisfactory results. The moving averages (3) that can be approximated by low-pass filters work well and are much more simple to implement.

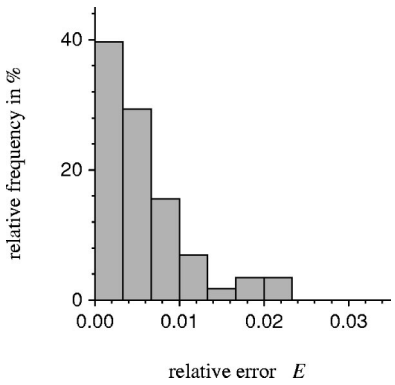

FIG. 3. Histogram of the relative error E of the determination of the unstable fixed-point intensities S_x^0 und S_y^0 from the moving averages $\langle S_x(t)\rangle$ and $\langle S_y(t)\rangle$ of the uncontrolled system. The histogram has been calculated from the measurements of 58 unstable fixed points that could be stabilized at pump rates r with $1.9\leqslant r \leqslant 4$.

IV. CHARACTERIZATION OF THE STABILITY PROPERTIES OF THE STABILIZED UNSTABLE FIXED POINTS

In this section we describe the properties of the unstable steady-state solutions of the Nd:YAG laser. The implications of this investigation will affect the understanding of the control performance, i.e., when a stabilization can be achieved and how it should be done, e.g., which measurement signals should be fed back and which control parameters are appropriate. All results are obtained from the experiment looking at the behavior of the laser close to the unstable fixed point. So the reported results concerning the stability properties of the fixed points, their location and so on refer only to unstable fixed points that could be stabilized. The characterization of the unstable fixed points that could not be stabilized could not be done.

A. Influence of the control parameter

In order to describe the control performance the influence of the control parameter p on the laser system is important. For this purpose the effect of small changes of p on the location of the fixed point in the state space used for observing the system is crucial [7,17] for feedback control with small disturbances. As our observation space used for control in Eq. (2) is (S_x,S_y) the quantity of special interest in our case is

$$\mathbf{g}=\frac{\partial \mathbf{S}^0}{\partial p},$$

which describes the displacement of the unstable fixed point in the S_x-S_y plane under small changes of the control parameter. To determine $\mathbf{g}$ in our experiment we stabilized a fixed point at some injection current p_0 using Eq. (2). Then we raised p_0 for a short time by Δp_0 [see Fig. 4(b)]. If Δp_0 is

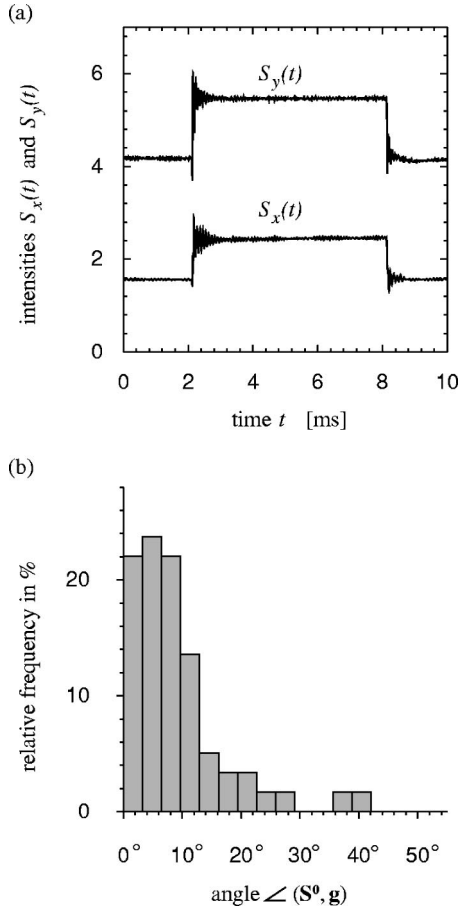

FIG. 4. Influence of the control parameter p. In (a) the intensities $S_x(t)$ and $S_y(t)$ are shown when the pump current is raised from 760 mA to 772 mA for a short time (6 ms); (b) histogram of the angle between the vector $\mathbf{S}^0$ and the corresponding displacement vector $\mathbf{g}$ (calculated from the measurements of 59 different stable and unstable fixed points with pump rates r between $1.9 \leqslant r \leqslant 4$).

not chosen too big the feedback loop still stabilizes the steady state. If the control signal continues to have zero mean the new position of the unstable fixed point at $p_0 + \Delta p_0$ can directly be measured. Due to the low-pass property of the bias tee this is allways the case in our experiment. Thus $\mathbf{g}$ can be approximated by

$$\mathbf{g} \approx \frac{\mathbf{S}^0(p_0+\Delta p_0)-\mathbf{S}^0(p_0)}{\Delta p_0}.$$

For stable fixed points $\mathbf{g}$ is calculated in the same way. But here of course no stabilization is needed.

The short lasting raise of the injection current leads in first approximation to an amplification of each laser mode. Therefore one can expect that the displacement vector $\mathbf{g}$ and the fixed-point vector $\mathbf{S}^0$ are almost parallel. In Fig. 4 the histogram of the angle between $\mathbf{S}^0$ and $\mathbf{g}$ calculated from the measurements of 59 stable and stabilized unstable fixed points is shown. As can be seen there are angles that exceed 0° by far, but most of the observed angles are less than 10°. Therefore in most cases the directions of $\mathbf{S}^0$ and $\mathbf{g}$ are very similar.

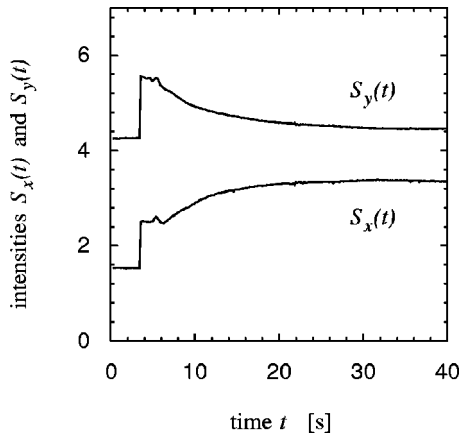

FIG. 5. A typical behavior of the intensities S_x and S_y of a steady state is shown when the injection current is raised from 760 mA to 772 mA for a long time period. The same initial steady state as in Fig. 4(a) is used.

This short-time behavior has to be destinguished from the case that the injection current is changed for a longer time period (see Fig. 5). In this case due to thermal effects it can happen that after a transient time some laser modes are damped although the injection current has been increased. In Fig. 5 we show starting from the same stable steady state as in Fig. 4(a) the behavior of S_x and S_y when the injection current is raised for a longer time. As can be seen at the beginning the same short-time behavior occurrs as in Fig. 4(a) but after about 2 sec thermal effects become valid and the intensities go to another final stable steady state. Therefore, for the determination of $\mathbf{g}$ used for feedback control with small, continuously changing control parameter, $\mathbf{g}$ has to be determined evaluating the short-time behavior in Fig. 4(a).

Slowly increasing the injection current leads in general to large variations of the relation of S_x^0 and S_y^0. To quantify this relation we use the angle α between $\mathbf{S}^0$ and the S_x axis [see Fig. 8(a) for visualization] defined by

$$\alpha = \arctan\frac{S_y^0}{S_x^0}. \tag{5}$$

This angle will play a major role in the characterization of the stability of the fixed point and our ability to stabilize it. In Fig. 6(a) the change of the angle α is plotted against the slowly increasing injection current. Depending on the position of the KTP crystal the outcome of this experiment can look totally different. But typical is that α does not stay constant but changes remarkably over a whole range while the total intensity S_{tot}^0 raises almost linearly with the injection current [see Fig. 6(b)].

B. The unstable direction

In the laser system the stable steady state usually loses its stability due to a Hopf bifurcation. Therefore it is expected that the unstable subspace is at least two dimensional and the

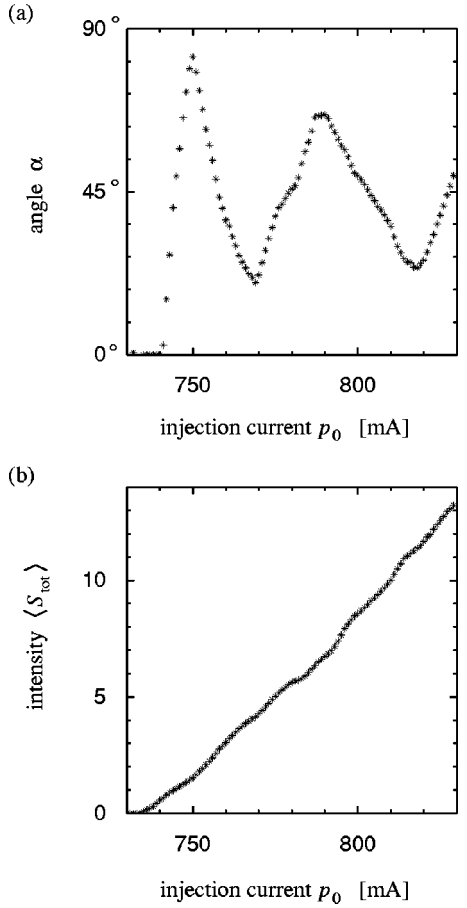

FIG. 6. Typical behavior of the steady-state position during increasing the injection current from 730 mA to 830 mA: (a) angle $\alpha = \arctan\langle S_y \rangle / \langle S_x \rangle$ as function of the injection current p_0; (b) the corresponding total intensity $S_{tot}^0 \approx \langle S_{tot} \rangle$ of the steady state.

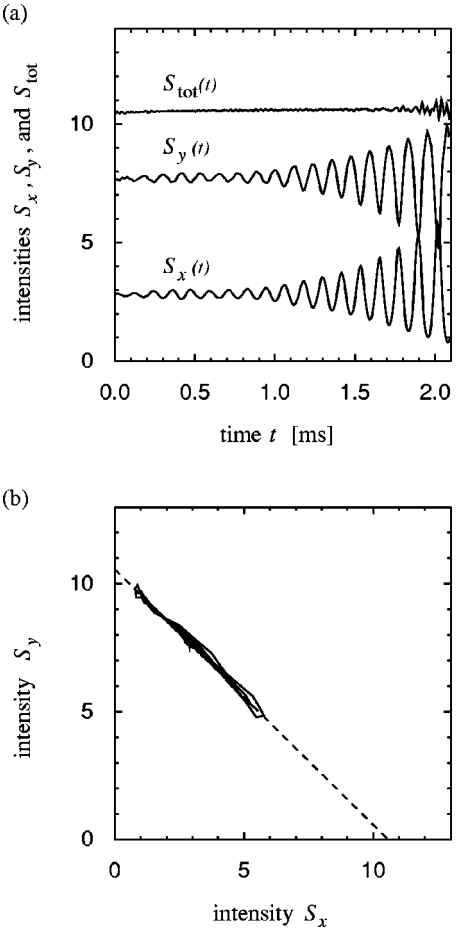

FIG. 7. Determination of the unstable direction. In (a) and (b) the typical behavior of $S_x(t)$, $S_y(t)$, and $S_{tot}(t)$ is shown after having stopped the stabilizing control signal (measurements taken at $r = 1.9$). The dotted line in (b) corresponds to S_{tot} being constant.

unstable eigenvalues are complex so that the unstable behavior can be linearly described by the trajectory spiraling away from the fixed point.

Now, the determination of the unstable direction is done by stabilizing a fixed point and observing the behavior of the system just after the control has been stopped.

In Fig. 7(a) the resulting behavior of $S_x(t)$, $S_y(t)$ and $S_{tot}(t) = S_x(t) + S_y(t)$ is plotted as a function of time. The increasing oscillations are clearly visible in $S_x(t)$ and $S_y(t)$ but hardly in $S_{tot}(t)$. This fact becomes also evident in the S_x-S_y plane in Fig. 7(b). The dotted line there coresponds to a constant total intensity.

This behavior seen in Fig. 7 is typical of the unstable fixed points of the laser. It has been observed for 48 fixed points (see Fig. 8) at different positions in the S_x-S_y plane described by the angle α (5), $\alpha \in [9°, 81°]$, and different pump rates ($r \in [1.9, 4]$). In Fig. 8(a) the behavior after stopping control is schematically visualized. In the S_x-S_y plane the trajectory performs an elliptical spiral with principal axes of length w_1 and w_2. The relation of the length of these axes w_2/w_1 is very small such that the projection of the unstable subspace into the S_x-S_y plane seems to be quasi-one-dimensional. The quotient w_2/w_1 has been determined for the 48 fixed points by calculating the singular values w_1 and w_2 of the matrix

$$\begin{pmatrix} \delta S_x(t_1) & \delta S_y(t_1) \\ \delta S_x(t_2) & \delta S_y(t_2) \\ \vdots & \vdots \\ \delta S_x(t_N) & \delta S_y(t_N) \end{pmatrix} \tag{6}$$

with $\delta S_x(t) = S_x(t) - S_x^0$ and $\delta S_y(t) = S_y(t) - S_y^0$. The time t_N has to be chosen not too large so that one stays in the linear regime. In the experiment the average of the 48 values of w_2/w_1 yielded

$$\left\langle \frac{w_2}{w_1} \right\rangle \approx 0.066 \pm 0.025.$$

So, indeed, the projection of the unstable subspace in the S_x-S_y plane is quasi-one-dimensional. Furthermore the direction of this projection was found to be almost independent of the position of the fixed point given by α and the pump rate r. To describe this direction we use the angle χ [see Fig. 8(a)] between the S_x axis and the main axis of the spiraling

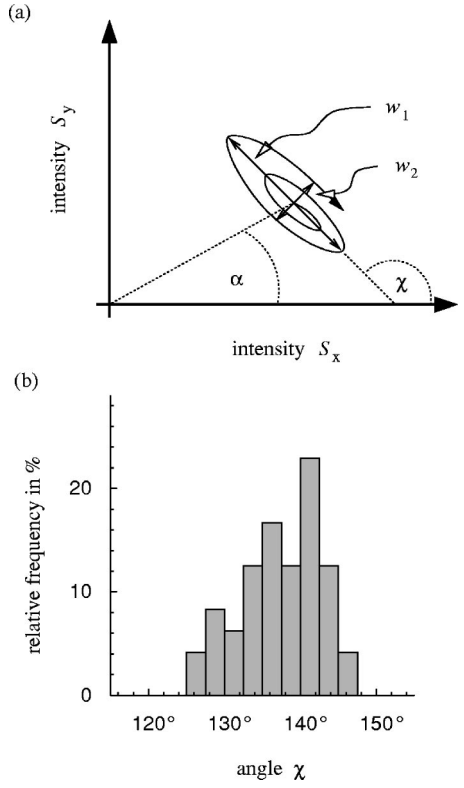

FIG. 8. Determination of the unstable direction. In (a) the typical behavior of destabilization of an unstable fixed point is schematically described and the definitions of w_1, w_2 and the angles χ and α is are presented. In (b) the histogram of the angle χ is shown. It has been calculated from the measurements of 48 unstable fixed points with $r \in [1.9,4]$ and $\alpha \in [9°,81°]$.

trajectory. For its determination again the singular value decomposition of the matrix (6) is used. χ can be calculated from

$$\chi = \arccos[(1,0) \cdot \mathbf{v}_1] \tag{7}$$

with $\mathbf{v}_1$ being the singular vector belonging to the largest singular value w_1. For the 48 fixed points this determination gives an averaged value

$$\langle \chi \rangle \approx (137.3 \pm 5.5)°.$$

In Fig. 8(b) the histogram of the angle χ is shown. For $\chi = 135°$ and $w_2/w_1 = 0$ the projection of the unstable subspace in the S_x-S_y plane would be exactly one dimensional and such that changes in the unstable subspace would not affect $S_{\mathrm{tot}} = S_x + S_y$ [see for comparison Fig. 7(a)]. The observed behavior for 48 fixed points shows that this scenario is a quite good description of the typical property of the unstable direction. This means that when a fixed point destabilizes, $S_{\mathrm{tot}} = S_x + S_y$ remains almost constant. Therefore S_{tot} is not a suitable input for the feedback control as the destabilization cannot be observed with S_{tot}.

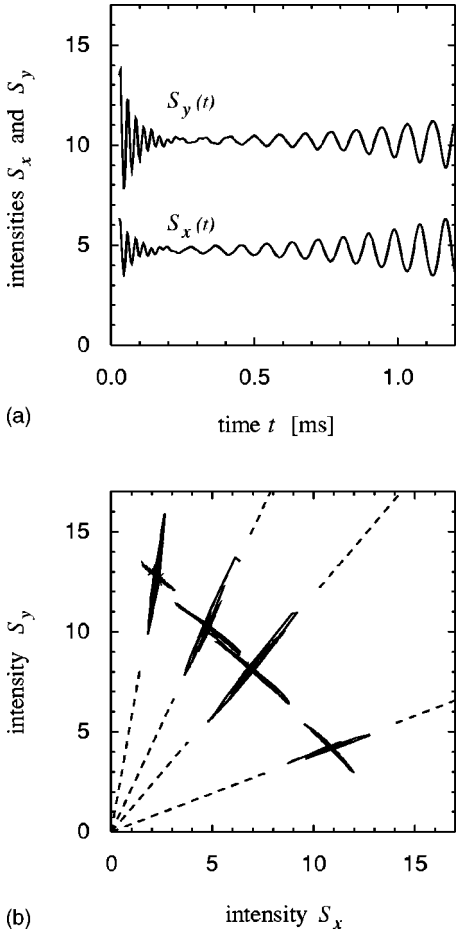

FIG. 9. Behavior of S_x and S_y starting close to the stable subspace of a fixed point. (a) S_x and S_y with respect to time; (b) The corresponding trajectories in the S_x-S_y plane. The dotted lines indicate the direction that is defined by the corresponding fixed point $(S_x^0, S_y^0)^{\mathrm{tr}}$.

C. The stable direction

Since the feedback control generally influences not only the unstable directions but also the stable direction one has to determine the stable subspace from the observation of the uncontrolled system. Normally, the unstable subspace influences the dynamics in the vicinity of an unstable fixed point so much, that the stable dynamics is hardly observable. To observe the dynamics in the stable subspace the initial point has to be very close to the stable manifold and at the same time not too close to the fixed point in order to obtain measurable deviations. In Fig. 9(a) the behaviors of the intensities $S_x(t)$ and $S_y(t)$ starting from such an initial point are shown. First the oscillation amplitudes decrease due to the influence of the stable direction. After a short time period the amplitudes increase caused by the unstable dynamics. The frequency of the increasing oscillations is clearly different from the decreasing oscillations.

To observe this behavior shown in Fig. 9 we applied the control signal (2) using large feedback parameters k_x and k_y near the margin of the stability regime. Doing so we were able to stabilize periodic behavior with small amplitudes near the unstable fixed point. After switching off the control,

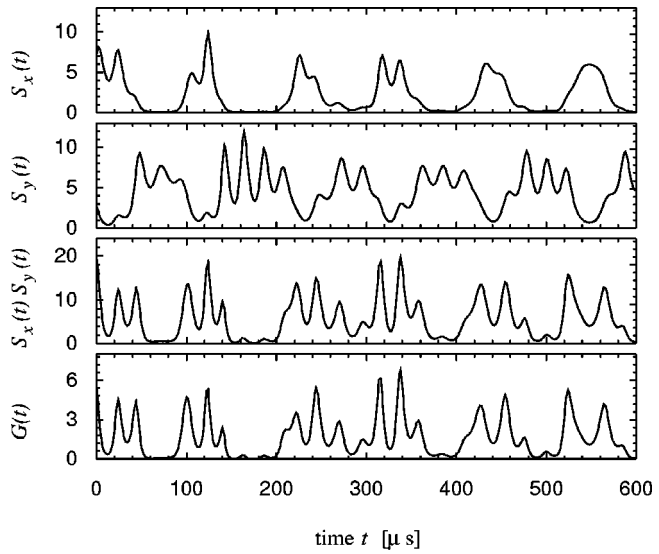

FIG. 10. Comparison of the green intensity $G(t)$ with the product of the infrared intensities $S_x(t)$ and $S_y(t)$. The intensities are measured at the pump rate $r=2.5$.

first the stable direction and then the unstable direction could be observed. In Fig. 9(b) four examples are shown in the S_x-S_y plane. The dotted lines indicate the direction defined by the corresponding fixed point (S_x^0,S_y^0).

This plot gives rise to the assumption that the stable subspace is also at least two dimensional and the projection on the S_x-S_y plane is quasi-one-dimensional. In contrast to the projection of the unstable subspace the projection of the stable subspace depends on the position of the fixed point. It seems to be approximately parallel to the vector (S_x^0,S_y^0).

D. The green intensity

Here we investigate whether the green intensity $G(t)$ is able to observe the dynamics of the laser in the unstable subspace of the fixed points. First we note, that the green intensity $G(t)$ is related to the product of the two orthogonal polarized infrared intensities $S_x(t)$ and $S_y(t)$. In Fig. 10 the similarity of $G(t)$ and $S_x(t)S_y(t)$ is obvious. So we make the approximation

$$G(t)\approx v S_x(t)S_y(t) \tag{8}$$

with some proportionality factor v. The type II phase matching of the KTP crystal makes Eq. (8) plausible as the phase matching is done such that the orthogonal polarized infrared modes interfere in an optimal way. The model equations in [18] also support this ansatz. This is somewhat in contrast to the experimental observation in [19], that the green intensity is proportional to the sum of S_x and S_y. This could not be observed in our experiment. Here, Eq. (8) holds very well as first approximation although it deteriorates when the pump rate is increased. Then more terms in Eq. (8) have to be considered.

An important difference between the green intensity and the infrared intensity is that the moving average of the uncontrolled system does not give an estimate of the value of

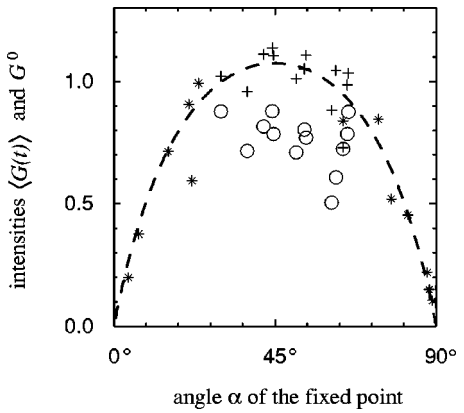

FIG. 11. Green steady-state intensities G^0 of stable (*) and unstable (+) fixed points for the pump rate $r=2.2$. For the unstable fixed points the averaged green intensities $\langle G(t)\rangle$ (○) of the uncontrolled laser are lower than the corresponding steady-state intensities. The dashed line is calculated from Eq. (8) using a fitted factor v.

the green intensity G^0 of the unstable fixed point. This is an immediate consequence of Eq. (8). In general it holds

$$G^0\approx p\langle S_x(t)\rangle\langle S_y(t)\rangle\neq p\langle S_x(t)S_y(t)\rangle\approx\langle G(t)\rangle.$$

For our laser system where typically only one intensity $S_x(t)$ or $S_y(t)$ is clearly different from zero at an arbitrary time t (see Fig. 10) one can conclude that the average intensity $\langle G(t)\rangle$ is smaller than the intensity of the unstable fixed-point G^0. This can be verified in the experiment. In Fig. 11 the green intensity G^0 of the steady state is shown in dependence of the angle α for a fixed pump rate $r=2.2$. The different angles α are obtained by positioning the KTP crystal differently. For the angles $\alpha<30°$ and $\alpha>75°$ only stable steady states could be observed at this pump rate. In this region states in between periodic and chaotic states could be found. In this region the averaged green intensity $\langle G(t)\rangle$ of these states is lower than the green intensity G^0 of the stabilized unstable fixed point. Therefore stabilizing the laser system leads here to increasing the green output of the frequency doubled Nd:YAG laser.

Now we come to the question, whether the green intensity is well suited to observe the unstable direction of the fixed point. To this end we must look at the behavior of G in the neighborhood of the fixed point, i.e., at $\delta G(t)=G(t)-G^0$. In linear approximation around $(S_x^0,S_y^0)^{\mathrm{tr}}$ the quantity $\delta G(t)$ can be calculated from Eq. (8) as

$$\delta G(t)\approx v(S_y^0,S_x^0)\begin{pmatrix}\delta S_x(t)\\ \delta S_y(t)\end{pmatrix}. \tag{9}$$

Following the results of our stability analysis in Sec. IV B for the unstable direction the approximation $\delta S_y(t)\approx-\delta S_x(t)$ holds [see Fig. 8(a)] that corresponds to $\chi=135°$. Inserting this in Eq. (9) yields

$$\delta G(t)\approx v(S_y^0-S_x^0)\,\delta S_x(t)$$

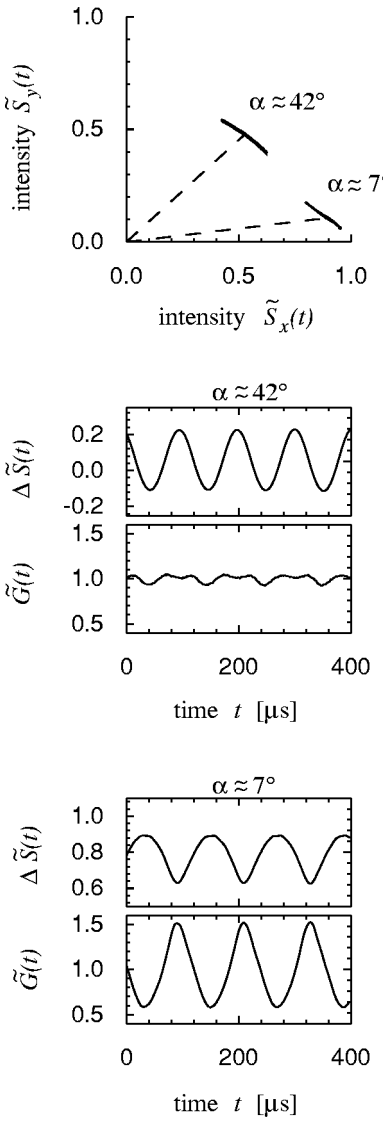

FIG. 12. Visibility of the unstable direction using the green intensity. The normalized infrared intensities $\Delta\tilde{S}(t)=\tilde{S}_x(t)-\tilde{S}_y(t)$ of two unstable fixed points ($\alpha\approx 7°$, $r=4.0$ and $\alpha\approx 42°$, $r=1.9$) are compared with the normalized green intensity $\tilde{G}(t)$. In both cases the laser fulfills small oscillations in the unstable subspace.

when the system destabilizes along the unstable direction. Therefore, in this case for $S_y^0=S_x^0$ ($\alpha=45°$), we do not expect to see large fluctuations of the green intensity. The amplitude of the fluctuations should be maximal for $S_x^0=0$ or $S_y^0=0$, i.e., for $\alpha=90°$ or $\alpha=0°$ respectively.

To check this in the laser experiment, measurements at 30 different fixed points have been performed for pump rates $1.74\leqslant r\leqslant 4.1$. As the range of the measured intensities are quite different we use in the following the normalized quantities:

$$\tilde{S}_x(t)=\frac{S_x(t)}{\langle S_{\mathrm{tot}}(t)\rangle}, \tag{10}$$

$$\tilde{S}_y(t)=\frac{S_y(t)}{\langle S_{\mathrm{tot}}(t)\rangle}, \tag{11}$$

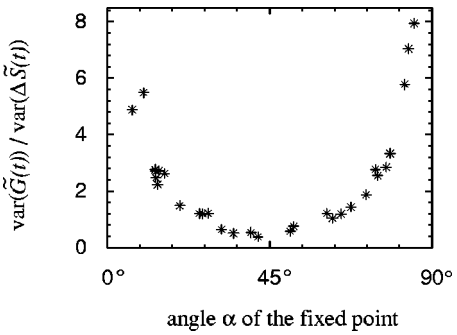

FIG. 13. For 30 fixed points at pump rates $1.74\leqslant r\leqslant 4.1$ var$[\tilde{G}(t)]$/var$[\Delta\tilde{S}(t)]$ is plotted versus α as a measure of how well the unstable direction can be observant using the green intensity.

$$\tilde{G}(t)=\frac{G(t)}{\langle G(t)\rangle}. \tag{12}$$

As the intensities $\tilde{S}_x(t)$ and $\tilde{S}_y(t)$ oscillate almost in antiphase in the unstable subspace the quantity $\Delta\tilde{S}(t)=\tilde{S}_x(t)-\tilde{S}_y(t)$ is well suited to observe the unstable direction.

In order to measure the unstable direction in the experiment the same procedure as described in Sec. IV B would be natural, i.e., measuring $S_x(t)$, $S_y(t)$, and $G(t)$ just after having stopped the control. But with our experimental setup it is not possible to observe three measurement signal in the control modus. Therefore we chose the following approach. By properly positioning the KTP crystal and the pump rate r we found 30 fixed points just after they had gone through a Hopf bifurcation. At this point the laser fulfills small periodic oscillations in the unstable subspace. In Fig. 12 two of these measurements are shown. One measurement was taken for a fixed point with α about 42° and the other with α about 7°. As expected from Eq. (9) for $\alpha\approx 42°$ the unstable direction cannot be observed very well with the green intensity while for $\alpha\approx 7°$ the unstable direction is clearly visible in the oscillations of the green intensity.

In Fig. 13 the results for the 30 fixed points are summarized in one plot. As a measure for quantifying how well the fluctuations in the unstable directions can be observed with the green intensity compared to $\Delta\tilde{S}$ we chose var$[\tilde{G}(t)]$/var$[\Delta\tilde{S}(t)]$. This quantity is shown in Fig. 13 versus α. From this plot it is obvious that for $\alpha\approx 45°$ the green intensity is not a good quantity to be used in a feedback loop as the dynamics in the unstable direction does hardly affect the green intensity.

E. Summary and consequences for the control method

First of all, we found that the infrared steady-state intensities that are essential for the feedback formula (2) can be approximated by the averaged intensities of the uncontrolled system. This can be realized by simple low-pass filters. Second, we found general features for the stability properties of the fixed points we were able to stabilize. So, we observed that both the stable and unstable subspace of the fixed point

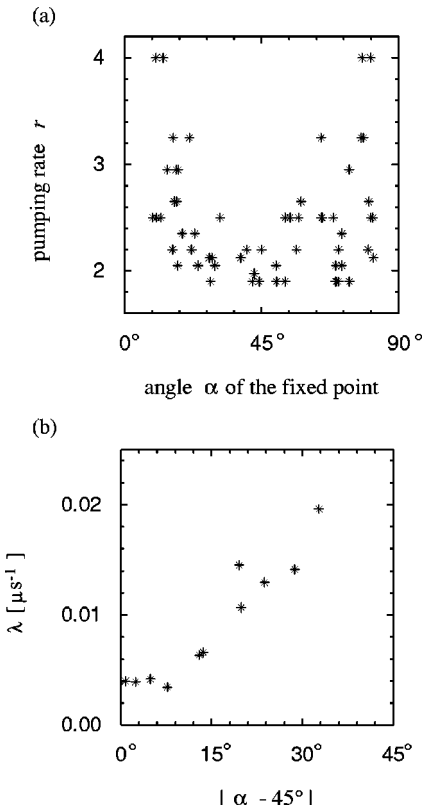

FIG. 14. In (a) the pump rates r of 59 stabilized unstable fixed points vs the angle α of the fixed points are shown. For these fixed points the eigenvalues of the linearization of the flow have been calculated. In (b) the maximal value of the real parts of these eigenvalues found for each α is plotted vs $|\alpha-45°|$. It is visible that the fixed points that could be stabilized near 45° are not very unstable.

have quasi-one-dimensional projections in the S_x-S_y plane. For the characterization of the fixed point the angle $\alpha = \arctan(S_y^0/S_x^0)$ proved to be very helpful. The unstable direction is independent of the angle α and is approximately given by the vector $(1,-1)^{\mathrm{tr}}$ in the δS_x-δS_y plane. An immediate consequence is that the total infrared intensity S_{tot} is not a suitable measurement signal for control. This explains why type II chaos could not be stabilized in [8,9] because there S_{tot} was used as input for the OPF control method. In contrast to the unstable direction we found that the stable direction is almost parallel to the fixed-point vector $\mathbf{S}_0$ and is given by α.

The displacement vector $\mathbf{g}$ which is a measure of the influence of the control parameter is also parallel to $\mathbf{S}_0$ when the injection current is used as control parameter. As the control should ideally only influence the dynamics of the unstable direction, the injection current is not appropriate for control because the angle between $\mathbf{g}$ and the stable direction is very small.

We could not stabilize the laser for high pump rates using the injection current as control parameter, and especially for $\alpha=45°$ it was even more difficult (see Fig. 14) if not impossible to achieve a stabilization. For the ordinary differential equation (ODE) investigated in [12] one can analytically show that it is impossible to stabilize a fixed point with $S_x^0 = S_y^0$, i.e., $\alpha=45°$ using the pump rate as control parameter [20].

In [20] we numerically investigated the properties of the unstable fixed points for 1710 different laser configurations where up to 20 laser modes and pump rates up to 10 were used. All the observations made in the experiment could be confirmed. For the projection of the unstable direction in the S_x-S_y plane these investigations yielded

$$\langle \chi \rangle \approx (135 \pm 0.07)°$$

and

$$\left\langle \frac{w_2}{w_1} \right\rangle \approx 0.03 \pm 0.017.$$

For the stable direction one obtained

$$\langle \beta - \alpha \rangle \approx (0 \pm 0.37)°,$$

where β is the angle enclosed by the stable direction and the S_x axis. In this numerical analysis we also determined the relation w_2/w_1 of the length of the principal axes for the stable direction. We obtained as averaged value

$$\left\langle \frac{w_2}{w_1} \right\rangle \approx 0.0125 \pm 0.0054.$$

Also the influence of the control parameter (in the ODE the pump rate) is similar as in the laser experiment. The investigation in the model equations gave

$$\langle \angle(\mathbf{g}, \mathbf{S}^0) \rangle = \left\langle \arctan \frac{g_y}{g_x} - \alpha \right\rangle \approx (0 \pm 0.28)°,$$

which means that the injection current influences mainly the dynamics of the stable subspace

V. CHOICE OF THE FEEDBACK PARAMETERS k_x AND k_y

In order to automatically determine suitable parameters k_x and k_y of the feedback loop (2) and to adapt them during control we first define a measure for the performance of the feedback control. We call this measure the cost function of our control method.

We distinguish two cases for choosing the feedback parameters k_x and k_y. When starting to control a fixed point one has to find the region in the k_x-k_y plane where most probably the feedback loop will be able to stabilize the fixed point. This we do taking into account what we have learned about the stability directions of the fixed points. The second case refers to the adaptation of the parameters during control which is always necessary because of drifting parameters of the laser experiment that reflects the tendency of the laser to behave instationarily. For the slight adaptation of the parameters we use simulated annealing for optimizing the cost function that we define now.

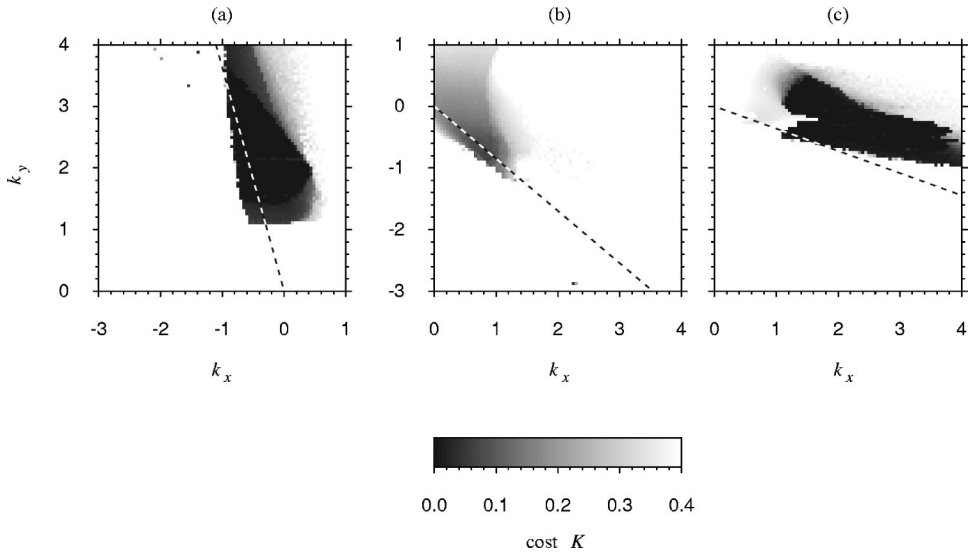

FIG. 15. The cost function K in dependence of the feedback parameters k_x and k_y at $r=2.5$. The function is gray coded; light gray refers to high costs and dark gray to small costs. In (a) $S_x^0/S_y^0 \approx 4.2$, in (b) $S_x^0/S_y^0 \approx 0.85$, and in (c) $S_x^0/S_y^0 \approx 0.35$. The dotted lines reflect the relation $k_x S_x^0 = -k_y S_y^0$ [see Eq. (16)] that is deduced considering the stability direction of the fixed point.

A. Definition of a cost function

Our cost function K depends on the fluctuations of both infrared intensities S_x and S_y. This is in contrast to other measures of the control performances as, e.g., used in [8], where the averaged applied control signal $\langle p \rangle$ is used as quality measure. As a simple ansatz the function $K_s = \sqrt{\mathrm{var}(S_x) + \mathrm{var}(S_y)}$ could be used. Here we prefer a more problem-adapted cost function that takes into account the following experimental observation. Just before suitable feedback parameters have been found the shape of the laser trajectory in the S_x-S_y plane is similar to a circle. If this is the case usually the feedback parameters k_x, k_y have only to be changed a little to achieve the stabilization of the fixed point. So we have to quantify both the amplitude of the deviation from the steady-state solution and the discrepancy from a circle. To this end, we calculate the two-dimensional distance (radius)

$$R(t) = \sqrt{[S_x(t) - \langle S_x \rangle]^2 + [S_y(t) - \langle S_y \rangle]^2}$$

from the estimated steady state $(\langle S_x \rangle, \langle S_y \rangle) \approx (S_x^0, S_y^0)$. Now, the averaged radius $\langle R \rangle$ is a measure of the amplitude of the deviation and the discrepancy from a circle can be characterized by the standard deviation $\mathrm{var}(R)^{1/2}$. Hence, we use the normalized sum

$$K = \frac{\langle R \rangle + \mathrm{var}(R)^{1/2}}{\langle S_x \rangle + \langle S_y \rangle} \tag{13}$$

as cost function K that is normalized to the averaged total infrared intensity $\langle S_x \rangle + \langle S_y \rangle$.

B. Taking the stability directon into account

The investigation of the stability directions of the fixed point in Sec. IV showed that the projection of its stable and unstable subspace in the δS_x-δS_y plane is quasi-one-dimensional. In this idealization the unstable direction is given by the vector $(1,-1)^{\mathrm{tr}}$ independent of the angle α of the fixed point. The stable direction is approximately given by the fixed-point vector $(S_x^0, S_y^0)^{\mathrm{tr}}$.

Now, for choosing the parameters of the feedback loop the idea is not to disturb the laser system in its stable subspace as the system there is already well behaving and in the worst case one could even destabilize this stable behavior. Therefore we choose to feed back only the component of $(\delta S_x, \delta S_y)^{\mathrm{tr}}$ whose projection on the stable direction is zero. This component can be calculated using the vector $\mathbf{n}$,

$$\mathbf{n} = \frac{1}{\sqrt{(S_x^0)^2 + (S_y^0)^2}} (-S_y^0, S_x^0)^{\mathrm{tr}}, \tag{14}$$

which is orthogonal to our idealized stable direction $(S_x^0, S_y^0)^{\mathrm{tr}}$ in the δS_x-δS_y plane.

So, the feedback control (2) results in

$$\delta p(t) = k \mathbf{n}^{\mathrm{tr}} \delta \mathbf{S}(t) = \frac{k}{\sqrt{(S_x^0)^2 + (S_y^0)^2}} (-S_y^0, S_x^0) \begin{pmatrix} \delta S_x(t) \\ \delta S_y(t) \end{pmatrix}. \tag{15}$$

This equation now depends only on a single parameter k. Comparing it to Eq. (2) one finds that the parameters k_x and k_y obey the relation

$$k_x S_x^0 = -k_y S_y^0. \tag{16}$$

As can be seen the two intensities S_x and S_y have to be fed back with opposite signs to the pump current. The experimental observations show that in almost all cases the coupling parameter of the smaller intensity has to be positive. Therefore for $S_x^0 > S_y^0$ we choose k positive in Eq. (15). Starting with $k=0$ we increase k till we find a minimum of the cost funtion with $K \ll 1$. With this procedure we can find a region in the k plane with small costs and thus good performance of the feedback control. This can be seen in Fig. 15. The dotted lines reflect the relation (16). Furthermore, Figs. 15(a) and 15(c) reveal that the lines are not located in the

center of the stabilizing region. Furthermore, the negative k value [k_x in Fig. 15(a) and k_y in Fig. 15(c)] should be chosen a bit larger.

As a whole there are extended regions in the k plane that lead to a stabilization of a steady state of the laser. Our approach using Eq. (15) achieves stabilization quite well if S_x^0 and S_y^0 are not to similar and therefore α is not too close to 45°. But we occasionally found also examples where both k parameters had to be chosen positive. In these cases the just described procedure fails and the search for the appropriate feedback parameters has to be done by an alternative method that is described next.

C. Using simulated annealing

This method is used in cases where either Eq. (15) cannot achieve control or the adaptation of the parameters during control is needed due to the instationarity of the laser.

Having defined the cost function K, the simulated annealing proceeds as follows to find a minimum of K. Starting with the parameters (k_x,k_y) used in the feedback loop, successively new parameters $(k_{x,\mathrm{new}},k_{y,\mathrm{new}})$ are chosen at random in the vicinity of (k_x,k_y) and plugged into the feedback loop. Let the cost function before the modification be K_{old}, and after the exchange K_{new}. The modification will be accepted if it yields a lower value for the cost function, otherwise it will be changed with probability

$$p=\exp(-\Delta K/T),\ \Delta K=K_{\mathrm{new}}-K_{\mathrm{old}}.$$

The new parameters $(k_{x,\mathrm{new}},k_{y,\mathrm{new}})$ are then used as starting parameters for the next modification. If the modification is rejected the procedure is repeated using a different pair of parameters chosen in the vicinity of the unchanged parameters (k_x,k_y). This updating scheme was proposed by Metropolis *et al.* [21] to keep a system in equilibrium at a given temperature T. For minimization of the cost function K, the temperature T is lowered slowly [22]. Here we use a cooling scheme as proposed for example in [23]. The temperature T is lowered by a constant factor $\sigma<1$ to σT after N considered modifications or after N_{acc} accepted updates. Slower cooling in general leads to better minimization of K at the expense of time.

D. Tracking the unstable fixed point

The simulated annealing optimization is designed to handle small changes of the dynamics of the laser during control. Such a change is usually the result of the instationarity of the system. However, such changes can also be generated by increasing the injection current by a small amount. Maintaining the stabilization while changing a system parameter is the main idea of the tracking procedure of Schwartz and Triandaf [24]. They propose to stabilize an unstable fixed point and then to slowly alter a system parameter while adjusting the parameters of the feedback control such that the fixed point stays stabilized over the whole tracking process. The feasibility of the tracking idea has been demonstrated in different experiments. Using the OPF control a tracking process has been applied also to a frequency doubled Nd:YAG laser [8] in order to extend the range of stability of the steady state.

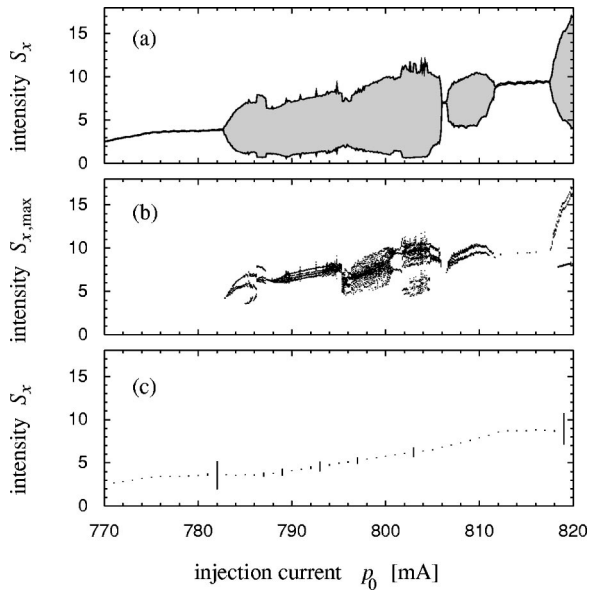

FIG. 16. Behavior of the intensity S_x increasing the injection current from $p_0=770$ mA to $p_0=820$ mA. In (a) and (b) the intensity fluctuation and the bifurcations diagram for the uncontrolled system are shown. The intensity fluctuation after each tracking step are shown in subfigure (c).

Having the simulated annealing optimization of the cost function at hand we are able to implement a robust tracking process in our laser system. Each time the injection current is increased by a small amount we start the simulated annealing optimization in order to find better feedback parameter k_x and k_y. Note that the position of the fixed points is automatically adapted by using Eq. (3). Furthermore, in contrast to the tracking process in [24,8] where the control signal is used as a measure for the control performance, we use here the cost function (13) based on the intensities S_x and S_y. Doing so we achieve keeping the system stabilized.

To demonstrate the feasibility of our tracking process we show in Fig. 16 the range of the intensity fluctuations of S_x as function of the injection current p_0 without control (a) and with activated control (c). For small p_0 no fluctuations occur. The system is stable without feedback control. To distinguish between the periodic and chaotic fluctuations of the uncontrolled system for larger p_0 we show in Fig. 16(b) the maxima $S_{x,\max}$ of an intensity time series recorded for each injection current $p_0=770,770.1,\ldots,820$. In Fig. 16(c) we recorded the intensity range after each optimization process that started just after the injection current was increased by 1 mA. In comparison to Fig. 16(a) the range of the fluctuations could be reduced significantly by this tracking process.

VI. SUMMARY AND CONCLUSIONS

We have demonstrated the successful stabilization of unstable fixed points of an intracavity frequency doubled Nd:YAG laser. We use a time-continuous linear feedback control with the two input variables S_x and S_y fed back to the

injection current of the pump diode. In contrast to preceding work we were able to stabilize the so called type II chaos where laser modes in both polarization eigendirections are present.

As main part of the paper we investigated carefully the stability properties of the unstable fixed points that we were able to stabilize. We found that the properties of the unstable fixed points could well be described in the S_x-S_y plane. First of all, the location of the unstable fixed points in the S_x-S_y plane can simply be approximated by the averaged intensities $\langle S_x \rangle$ and $\langle S_y \rangle$ of the uncontrolled system. The projection of the unstable subspace in the S_x-S_y plane is quasi-one-dimensional and in good approximation independent of the position of the fixed point. Its direction is close to the direction where the total intensity $S_{\mathrm{tot}}=S_x+S_y$ is constant. The projection of the stable subspace is quasi-one-dimensional too and can be approximated by the angle α between the S_x axis and the fixed point in the S_x-S_y plane. We also found that the influence of the injection current on the fixed points is nearly parallel to the stable direction.

The characterization of the properties of the stabilized fixed points leads to a good understanding of the control performance. The intensities S_x and S_y are good measurement quantities for the control, independent of the control strategy. In contrast, the total infrared intensity S_{tot} is not suited for control as fluctuations in the unstable subspace do not significantly change this intensity. Similarly, the green intensity G is also not suited for control. Particularly, when both intensities S_x^0 and S_y^0 of the fixed point are of the same order the unstable direction can hardly be observed using G.

Our investigations could be exploited to improve the process of finding appropriate proportionality factors k_x and k_y in the feedback loop. In addition, we also implemented a simulated annealing optimization of a cost function, based on the intensities S_x and S_y themselves as input. We applied a tracking process to the laser and could so extend the stability range of the steady state.

All in all, we found that our stabilization worked only for small pump rates $r \leqslant 4$. We explain this by the following two facts. First, the dead time of the DSP controller used to apply the feedback in our experiment has a bad influence on the stabilization performance, particulary for the more unstable fixed points at high pump rates. This effect can by minimized by building the controller using analog devices. Second, the injection current is a bad control parameter as it shifts the fixed point almost parallel to its stable direction. Thus the bad performance of the control is an inherent problem of a feedback control when the injection current is used as control parameter. This cannot be removed by changing the control formula. In the future, one should look instead for a better control parameter.

ACKNOWLEDGMENTS

A. S. would like to thank Professor W. Lauterborn and the nonlinear dynamics group at the Third Physical Institute for their support and stimulating discussions during his stay in Göttingen. We thank R. Pitka for his collaboration at the start of the lab experiment. We acknowledge instructive discussions with H. Halldorsson and R. Mehnert on different aspects of laser technology. We thank A. Kittel, F. Lange, T. Letz, and J. Parisi for fruitful collaboration. The present work was financially supported by the *Bundesministerium für Bildung, Wissenschaft und Technologie* (BMBF) under Contract No. 13N7037/8.

[1] T. Baer, J. Opt. Soc. Am. B **3**, 1175 (1986).
[2] H.D.I. Abarbanel, Z. Gills, C. Liu, and R. Roy, Phys. Rev. A **53**, 440 (1996).
[3] J.L. Nightingale *et al.*, Proc. SPIE **2986**, 86 (1997).
[4] R. Roy *et al.*, Phys. Rev. Lett. **68**, 1259 (1992).
[5] E.R. Hunt, Phys. Rev. Lett. **67**, 1953 (1991).
[6] B. Peng, V. Petrov, and K. Showalter, J. Phys. Chem. **95**, 4957 (1991).
[7] E. Ott, C. Grebogi, and J.A. Yorke, Phys. Rev. Lett. **64**, 1196 (1990).
[8] Z. Gills *et al.*, Phys. Rev. Lett. **69**, 3169 (1992).
[9] R. Roy, Z. Gills, and K.S. Thornburg, Opt. Photonics News **5**, 7 (1994).
[10] P. Colet, R. Roy, and K. Wiesenfeld, Phys. Rev. E **50**, 3453 (1994).
[11] T.W. Carr and I.B. Schwartz, Phys. Rev. E **51**, 5109 (1995).
[12] K. Pyragas *et al.*, Phys. Rev. E **61**, 3721 (2000).
[13] K. Pyragas, Phys. Lett. A **170**, 421 (1992).
[14] J.E.S. Socolar, D.W. Sukow, and D.J. Gauthier, Phys. Rev. E **50**, 3245 (1994).
[15] D.P. Lathrop and E.J. Kostelich, Phys. Rev. A **40**, 4028 (1989).
[16] K. Pawelzik and H.G. Schuster, Phys. Rev. A **43**, 1808 (1991).
[17] B. Hübinger *et al.*, Phys. Rev. E **50**, 932 (1994).
[18] C. Bracikowski and R. Roy, Chaos **1**, 49 (1991).
[19] F.G. Laeri *et al.*, Appl. Phys. B: Lasers Opt. **63**, 339 (1996).
[20] A. Schenck zu Schweinsberg, Dissertation, Der Andere Verlag, Osnabrück, 2000.
[21] N. Metropolis *et al.*, J. Chem. Phys. **21**, 1087 (1953).
[22] S. Kirkpatrick, Science **220**, 671 (1983).
[23] W.H. Press, S.A. Teukolsky, W.T. Vetterling, and B.P. Flannery, *Numerical Recipes in C* (Cambridge University Press, Cambridge, 1992).
[24] I.B. Schwartz and I. Triandaf, Phys. Rev. A **46**, 7439 (1992).